

The impact of a new
parametrization of turbulent
orographic form drag

Christian Keil and Anton Beljaars

Research Department

August 2003

*This paper has not been published and should be regarded as an Internal Report from ECMWF.
Permission to quote from it should be obtained from the ECMWF.*



European Centre for Medium-Range Weather Forecasts
Europäisches Zentrum für mittelfristige Wettervorhersage
Centre européen pour les prévisions météorologiques à moyen terme

For additional copies please contact

The Library
ECMWF
Shinfield Park
Reading
RG2 9AX
library@ecmwf.int

Series: ECMWF Technical Memoranda

A full list of ECMWF Publications can be found on our web site under:

<http://www.ecmwf.int/publications/>

©Copyright 2003

European Centre for Medium Range Weather Forecasts
Shinfield Park, Reading, RG2 9AX, England

Literary and scientific copyrights belong to ECMWF and are reserved in all countries. This publication is not to be reprinted or translated in whole or in part without the written permission of the Director. Appropriate non-commercial use will normally be granted under the condition that reference is made to ECMWF.

The information within this publication is given in good faith and considered to be true, but ECMWF accepts no liability for error, omission and for loss or damage arising from its use.

Abstract

A new method of parametrizing the effects of turbulent form drag due to subgrid orography in large scale models is evaluated conducting case-study-type and climate simulations with the ECMWF model. This part of the parametrization is traditionally represented by the effective roughness length concept and is assumed to represent horizontal scales up to 5 km. The performance is found to be slightly better than obtained with the effective roughness length parametrization. Comparisons with the MAP re-analysis and windprofiler observations show a small increase in wind speed and a clockwise rotation within the lowest kilometres for two MAP Intensive Observation Periods. The impact on the model climatology is found to be slightly beneficial compared against the present scheme and verified with ERA40 analysis. However, there is a strong compensation between the turbulent form drag and the gravity-wave drag schemes. The weak but favorable impact of the new scheme with its distributed drag is suggesting that this new approach is appropriate for mountainous areas. It is also important for a more general model development point of view as it decouples orographic drag from atmosphere to vegetation coupling.

1 Introduction

Turbulent form drag over land in numerical models is usually composed of the drag exerted by vegetation or buildings and the drag induced by subgrid-scale orography. Traditionally, the so-called effective roughness length (EFRL) concept has been used in numerical weather prediction (NWP) models whereby the vegetative roughness length is enhanced to account for the surface drag caused by the presence of the unresolved underlying orography. For this part of the drag horizontal scales up to 5 km are considered; subgrid scales above 5 km are represented by the gravity wave drag and low level blocking scheme (Lott and Miller, 1997). Such an approach has been justified by various numerical and experimental studies (Grant and Mason, 1990).

However, the concept does have a number of disadvantages. In mountainous terrain, the subgrid orography contributes substantially to the turbulent form drag and therefore the effective roughness length can reach several dekametres, larger than the thickness of lowest model layers. In turn, the transfer of scalars (e.g. temperature or humidity) is hardly affected by subgrid orographic effects and the roughness lengths for heat and moisture have to be reduced to compensate for the artificial enhancement of the aerodynamic roughness length.

A new scheme in which the effects of turbulent form drag caused by subgrid-scale orography are described by an explicit orographic stress profile has been suggested by Wood et al. (2001). To be practical in a NWP modelling context, Beljaars et al. (2003) simplified the turbulent orographic form drag scheme and made the new formulation applicable for a continuous range of scales.

In this paper the new turbulent orographic form drag parametrization is evaluated by performing a series of case-study-type simulations, long model integrations at reduced resolution to estimate the impact on the model climatology and an ensemble of full-resolution ten-day forecasts to be compared with current ECMWF operational scores. Two cases recorded during the Mesoscale Alpine Programme Special Observing Period (MAP SOP; Bougeault et al., 2001) are complemented by simulations of an episode observed in the Rocky Mountains which was previously investigated by Beljaars (2001).

The plan for the rest of the paper is as follows. Section 2 gives details of the new parametrization. Section 3 describes the simulations performed followed by the presentation and discussion of the results in sections 4 and 5. Conclusions are given in section 6.

2 The new turbulent orographic form drag parametrization

The novelty of the turbulent orographic form drag parametrization (TOFD) proposed by Beljaars et al. (2003) is the application of the explicit orographic form drag profile (Wood et al., 2001) for a continuous range of scales smaller than 5 km. The new elements of the parametrization are: (i) the spectrum of the orography is represented by a piecewise empirical power law, (ii) the turbulent form drag scheme integrates over the spectral orography to represent all the relevant scales, and (iii) the wind forcing level of the drag scheme depends on the horizontal scale of the orography, which implies that the small scales are shaded by the larger scales. Comparisons of single column simulations with output from fine scale simulations for sinusoidal hills show that the approximations are within the uncertainty of the fine scale models (Beljaars et al., 2003).

The parametrization developed can be summarized with the following set of equations

$$\frac{\partial}{\partial z} \bar{\tau}_o / \rho = -2\alpha \beta C_{md} C_{corr} |\bar{U}(z)| \bar{U}(z) \int_{k_o}^{k_\infty} \frac{k^2}{l_w} F_o(k) e^{-z/l_w} dk, \quad (1)$$

$$l_w = \min(2/k, 2/k_1),$$

with

$$\begin{aligned} F_o(k) &= a_1 k^{n_1}, \text{ for } k_o < k < k_1, \\ F_o(k) &= a_2 k^{n_2}, \text{ for } k_1 < k < k_\infty, \\ n_1 &= -1.9, n_2 = -2.8, \\ a_1 &= \sigma_{flt}^2 (I_H k_{flt}^{n_1})^{-1}, a_2 = a_1 k_1^{n_1 - n_2}, \\ k_o &= 0.000628 m^{-1}, k_1 = 0.003 m^{-1}, \\ k_{flt} &= 0.00035 m^{-1}, k_\infty = 2\pi c_m / z_o, \\ I_H &= 0.00102 m^{-1}, c_m = 0.1, \\ \alpha &= 12, \beta = 1, \\ C_{md} &= 0.005, C_{corr} = 0.6, \end{aligned} \quad (2)$$

where $k (= 2\pi/\lambda)$ is the wave number, k_o the lower bound of the integral set to half a wave length of 5 km, and $F_o(k)$ the variance spectrum of the orography. Parameter a_1 represents the spectral amplitude of the orography at scales of about 2 to 20 km and is determined from the available 1 km orographic data. σ_{flt} is the standard deviation of the filtered orography. A number of parameters (α , β , c_m , C_{md}) are only weakly dependent on the dimensions of topography and set constant. The correction factor C_{corr} has been determined using single column simulations.

The integral of the right hand side of Eq. (1) can be pre-computed for different heights, without giving a computational burden. However, with hybrid vertical coordinates (as in the ECMWF model), model level heights vary with surface pressure, and therefore it is more convenient to have an analytical expression. A good approximation of Eq. (1) is

$$\frac{\partial}{\partial z} \bar{\tau}_{xo} / \rho = -\alpha \beta C_{md} C_{corr} |\bar{U}(z)| \bar{U}(z) 2.109 e^{-(z/1500)^{1.5}} a_2 z^{-1.2}, \quad (3)$$

The use of Eq. (3) rather than (1) gives virtually identical results in single column simulations.

The two stress divergence expressions are included in the two components of the momentum equations and solved together with the turbulent diffusion equations. An implicit formulation is needed for stability. The standard way of time stepping a non-linear problem with implicit equations is by evaluating the non-linear part

at the old time level and keeping the linear part for the new time level. In this case it means that the absolute wind speed $|U|$ is taken from the old time level and that the $U(z)$ and $V(z)$ components are evaluated implicitly.

With Eqs. (3), and the constants in (2), the entire parametrization depends on a single geographical parameter namely the standard deviation of the filtered orography σ_{flt} . Because the software to compute σ_{flt} is not available yet, σ_{flt} has been set to $0.5 \times \sigma_{oro}$, where σ_{oro} is the standard deviation of subgrid orography as used by the gravity wave drag (GWD) and orographic blocking scheme. The coefficient has been optimized for data over the USA. With the new TOFD scheme the roughness lengths are set with a correspondence table linking them to vegetation type (Mahfouf et al., 1995).

3 Model experiment setup

The new TOFD is evaluated by performing case-study-type experiments (overview in Table 1 and results in section 4), experiments to assess the impact on the model climatology (overview in Table 2 and results in section 5) and a series of ten-days forecasts to validate the impact in terms of scores compared to current ECMWF operations.

The case-study-type and the ten-days forecast experiments are performed using the current operational resolution (T511L60), whereas the climate experiments are conducted on a reduced resolution (T95L60). For both model simulations of winter (DJF87/88) and summer (JJA87) climate an ensemble of 6 simulations are initialized on 01 Nov to 06 Nov 1987 (01 May to 06 May 1987, respectively) with a forecast range of 3000 hours. Note that no data assimilation is involved.

Table 1: List of ECMWF forecast experiments CY25R5 for MAP IOPs

expID	init. date	forecast time	used IFS binary	remarks
edvd	19xxxxxx12	+48 h	default	present effective roughness (EFRL)
ecxs	19xxxxxx12	+48 h	paa_CY25R5_tod2	new turbulent orographic drag (TOFD)
ed14	19xxxxxx12	+48 h	pal_CY25R5_notod	no TOFD scheme
ed18	19xxxxxx12	+48 h	pal_CY25R5_notod	no TOFD and GWD schemes

Table 2: List of ECMWF forecast experiments CY26R1: climate runs

expID	init. date	forecast time	used IFS binary	remarks
edz4	1987xx0112-0612	+3000h	pav_CY26R1_intsst	present EFRL scheme
ef01	1987xx0112-0612	+3000h	pal_CY26R1_tod2_tiles	new TOFD scheme
ef0a	1987xx0112-0612	+3000h	pal_CY26R1_notod	no TOFD scheme
ef6j	1987xx0112-0612	+3000h	pal_CY26R1_notod	no TOFD and GWD schemes

4 Case-study-type assessment

In this section, windprofiler observations recorded during two Intensive Observation Periods (IOP) of MAP SOP are used to assess the impact of the new turbulent orographic form drag parametrization (TOFD). Both IOPs represent different flow regimes: unblocked flow up and over the mountains during IOP2b and flow around or blocked during IOP8 (Keil and Cardinali, 2003). The two MAP cases are augmented with a case-study in the Rocky Mountains.

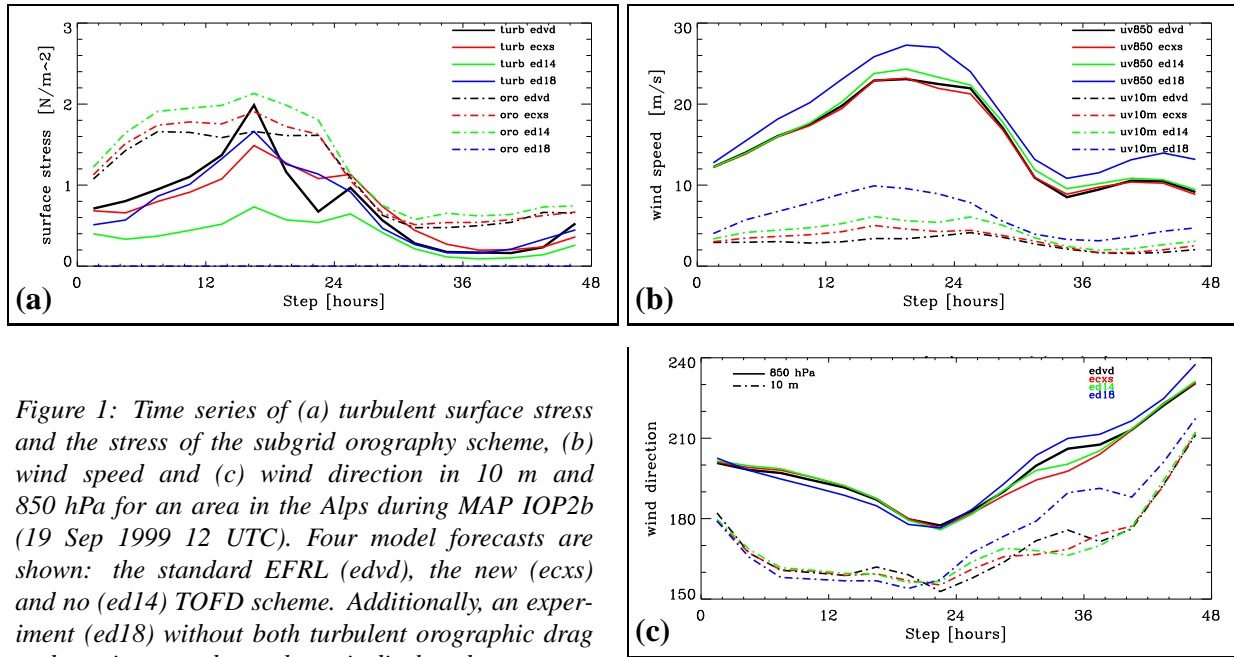


Figure 1: Time series of (a) turbulent surface stress and the stress of the subgrid orography scheme, (b) wind speed and (c) wind direction in 10 m and 850 hPa for an area in the Alps during MAP IOP2b (19 Sep 1999 12 UTC). Four model forecasts are shown: the standard EFRL (edvd), the new (ecxs) and no (ed14) TOFD scheme. Additionally, an experiment (ed18) without both turbulent orographic drag and gravity wave drag scheme is displayed.

During MAP, two windprofilers were operated at different frequencies (Very High Frequency VHF and Ultra High Frequency UHF) at Lonate close to Milan detecting vertical profiles of the flow field at different heights (VHF from ~ 2 km up to 15 km; UHF from a few hundred metres up to about 6 km. The measurements of both windprofilers are displayed using a tiling method which enables the depiction of the actually measured data without any field smoothing. The length of the individual tiles represents the frequency of the measurements reported by the windprofilers, with 1 hourly data from VHF Lonate and quarter-hourly data from UHF Lonate. Data sparse areas are also easy to identify. The corresponding analysis wind fields of the MAP re-analysis at Lonate are displayed using the same time-height representation.

4.1 MAP IOP2b

The atmospheric conditions prevalent during IOP2b (19-20 Sep 1999) constitute a 'prototype' case for intense weather in the Alpine region. Ahead of a baroclinic trough, a permanent northward flow has driven Mediterranean air towards the Alps. Before the arrival of the surface front on 20 Sep 12 UTC, wind and potential temperature have continuously increased upstream of the Alps. During IOP2b orographic enhanced heavy precipitation has been recorded at the southern Alpine slopes (Medina and Houze, 2003), while north of the Alpine chain strong föhn has been observed (Jaubert and Stein, 2003).

First, integral values of turbulent and subgrid orography stress for an area in the Alps (45.5 - 47.5 ° N and 7 - 14 ° E) illustrate the general behaviour of the different drag parametrization schemes (Fig. 1a). For the first 18 hours, the surface stress of the new TOFD is slightly smaller than those of the present TOFD. Consequently, the near-surface wind is stronger using the new TOFD (Fig. 1b). Thereafter, the ranking reverses, *i.e.* the surface stress of the new TOFD being slightly larger than the stress obtained with the standard EFRL. This is caused by a spin-up process: initially, the low-level wind using new TOFD exceeds the standard EFRL wind while the surface stress caused by new TOFD is smaller. This weaker turbulent orographic drag is compensated by stronger gravity-wave drag. However, the low-level wind further increases and eventually (after 18 hours) induces stronger surface stress exerted by the turbulent orographic drag. Consequently, the wind using new TOFD slows down and the gravity-wave drag becomes weaker.

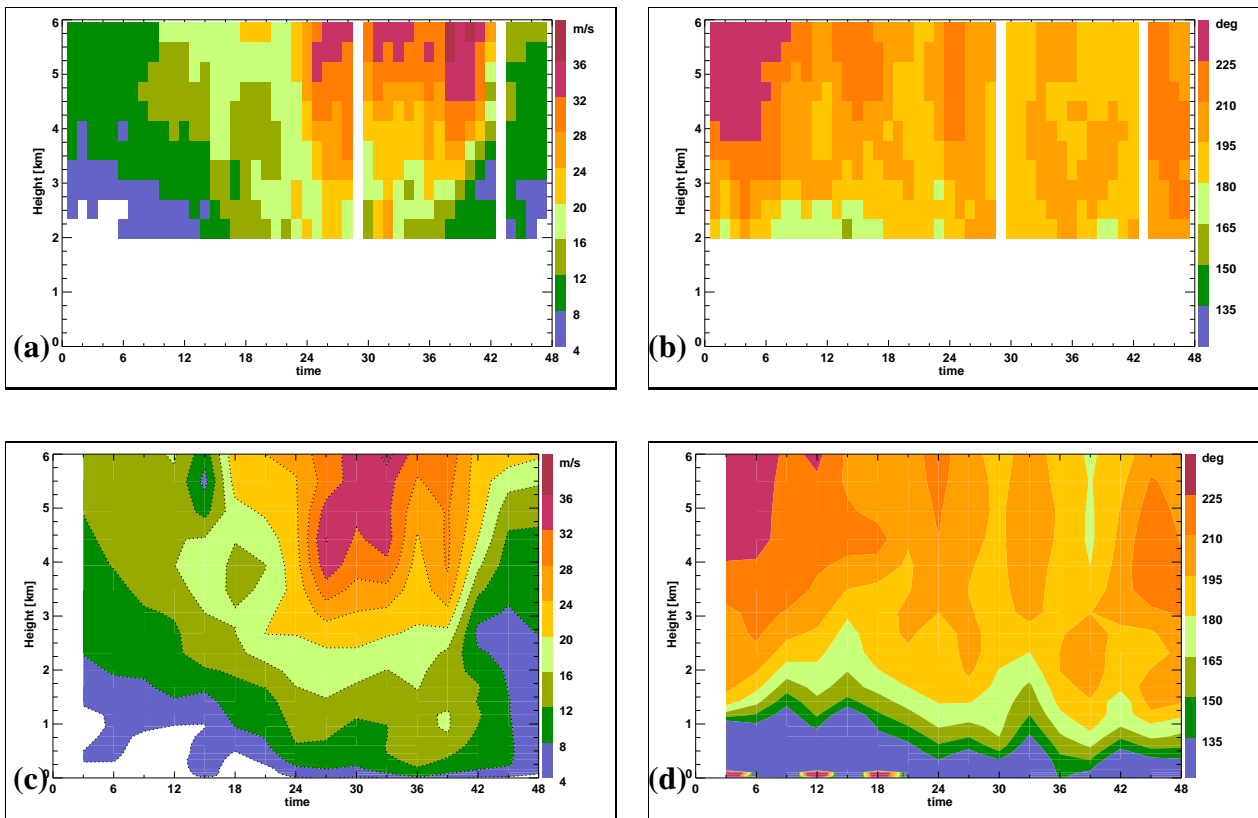


Figure 2: Time-height diagram (19 Sep 00 UTC till 21 Sep 00 UTC) of (a,c) horizontal wind velocity and (b,d) wind direction during IOP2b. The observations by VHF windprofiler at Lonate are shown in (a,b) and the corresponding analysis fields are shown in (c,d).

However, there is a strong compensation between the TOFD and the GWD scheme: smaller surface stress of the new TOFD causes higher surface stress exerted by the GWD scheme during the first 24 hours (red lines in Fig. 1), and vice versa (black lines). These compensating effects result in minor differences in wind speed of both experiments: the low-level wind of the new TOFD is slightly larger (≈ 1 m/s) whereas the wind in 850 hPa attains the same magnitude. Comparison of the wind direction shows no clear impact of the new scheme: wind from S to SE near the ground and from S to SW at 850 hPa (Fig. 1c). The strong compensation between both drag schemes becomes even more visible in two additional sensitivity experiments. Switching the TOFD off results in weak surface stress exerted by the vegetative component only and strong surface stress caused by the GWD scheme (green lines in Fig. 1). However, the GWD scheme is not totally compensating the lack of any TOFD which results in higher wind speed at low-levels and aloft. If both drag schemes are switched off, the surface stress exerted by the vegetation increases up to values of the TOFD, but since the GWD scheme is inactive, too, the wind increases in the entire boundary layer (blue lines).

Second, observed and reanalyzed wind speed and direction at Lonate located in the southern foothills of the Alps are compared with short-range forecasts using different drag parametrizations. The key feature of the wind profile observed with the VHF instrument at this southern Alpine windprofiler site is the strong pre-frontal jet attaining more than 20 m/s at 3 km height and more than 40 m/s above 4 km with a southwesterly direction (Fig. 2a,b). These observations were assimilated in the MAP re-analysis, which replicates the strong jet between 20 Sep 00 UTC and 18 UTC (+24 till +42 h in Fig. 2). The wind direction is rather constant in time with a strong rotation within the first two kilometres, corresponding to the barrier wind, an easterly wind present at low levels over the Po valley. Data from the UHF instrument, which records the profile from few

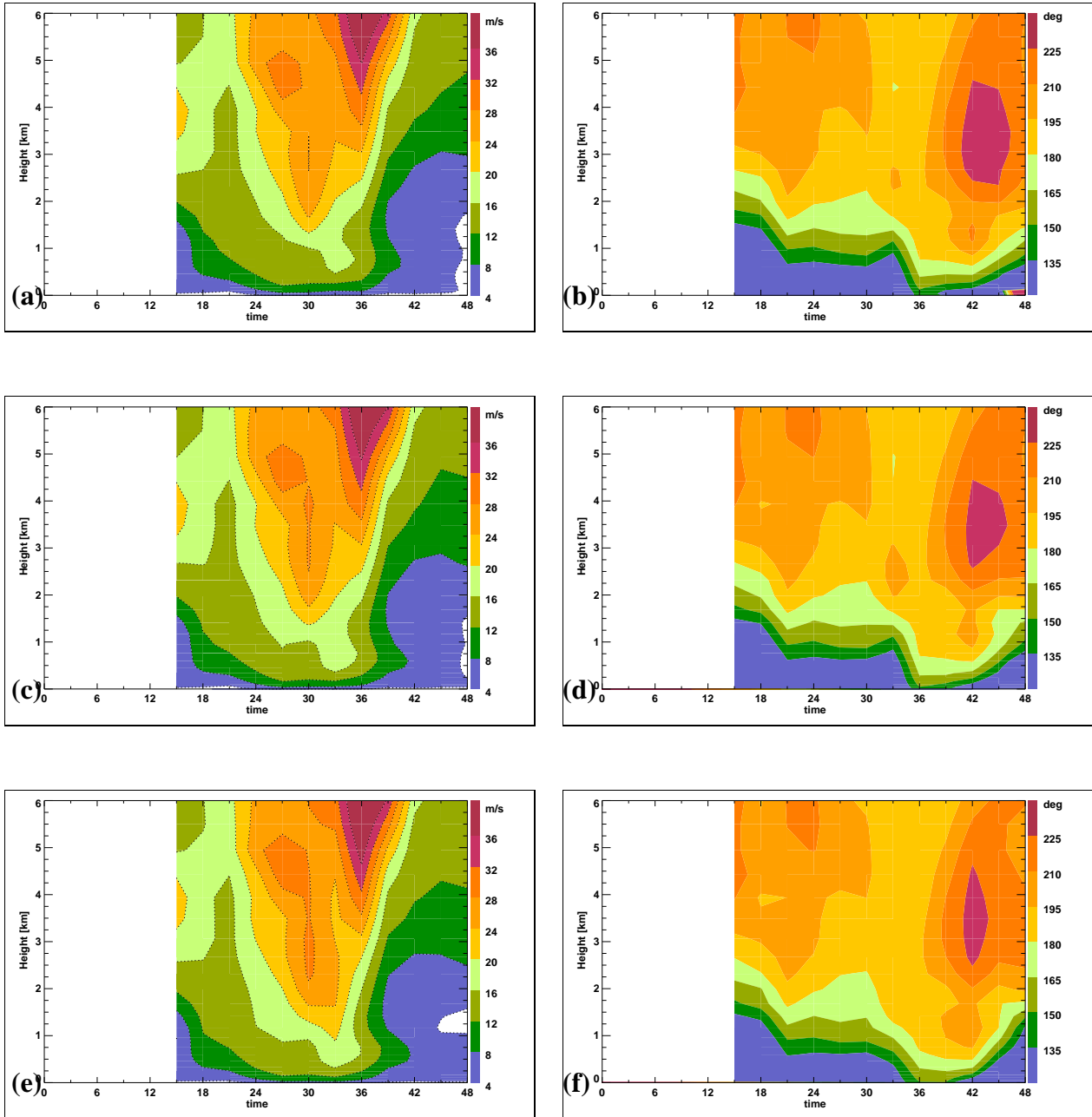


Figure 3: Time-height diagram (19 Sep 00 UTC till 21 Sep 00 UTC) of (a,c,e) horizontal wind velocity and (b,d,f) wind direction during IOP2b at Lonate: (a,b) CNTRL using present EFRL (edvd), (c,d) new TOFD (ecxs) and (e,f) without TOFD (ed14).

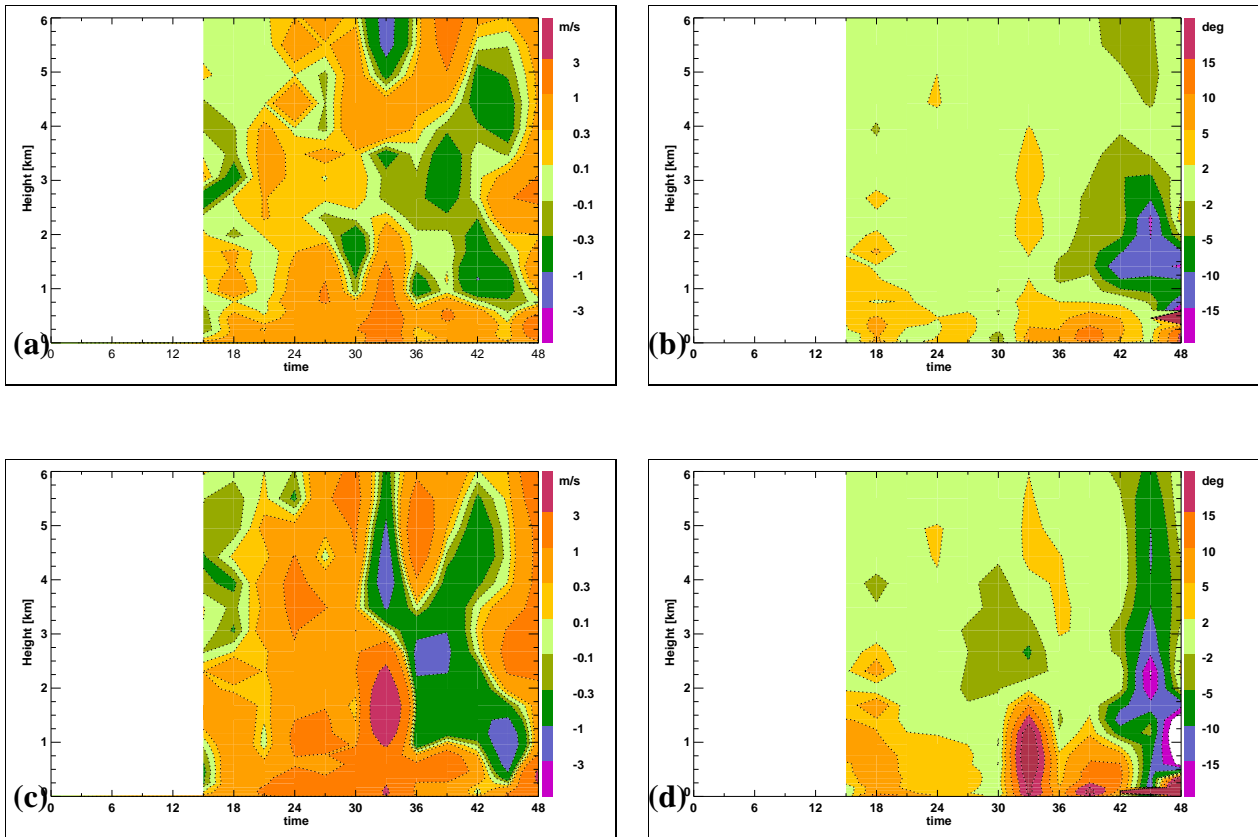


Figure 4: Differences of (a,c) horizontal wind velocity and (b,d) wind direction during IOP2b at Lonate displayed in a time-height diagram (19 Sep 00 UTC till 21 Sep 00 UTC) : (a,b) experiment using new TOFD minus CNTRL and (c,d) experiment without TOFD minus CNTRL.

hundred metres upwards, were not available at the MAP Data Centre for this case, unfortunately. However, Jaubert and Stein (2003) show UHF windprofiler data confirming the good quality of the reanalyzed wind speed and direction (their Fig. 3).

The temporal evolution of the wind profile computed using different drag parametrizations shows a satisfactory agreement for both wind speed and direction compared with observations and reanalyzed data (Figs. 2 and 3). The short-range forecasts capture the pre-frontal jet passage and the strong veering of the wind within the lowest kilometres with remarkable consistency. However, all forecasts overstate the depth of the jet. Below 3 km height, the model overestimates the wind speed by up to 10 m/s. The prevailing southwesterly to southerly wind direction above 2 km height and the strong rotation below, corresponding to the barrier wind, is reproduced. The bias between the short-range forecasts and the analysis can be estimated at about $15^\circ - 30^\circ$ over the vertical integral.

To assess the impact of the new scheme, three short-range forecasts are cross-compared (Fig. 4). Here the experiment with the standard EFRL serves as the reference, against which the new TOFD (Fig. 4a,b) and the no TOFD experiment (Fig. 4c,d) are compared. Using the new TOFD, the wind speed and direction is slightly enhanced (0.3 - 1 m/s and $5^\circ - 15^\circ$, respectively) within the lowest kilometre. Switching the TOFD off, leads to a further increase mainly confined to the lowest two kilometres. Unfortunately, the VHF windprofiler measures air motion above this height only. However, the differences between the short-range forecasts are within the range of the observation error of windprofiler observations.

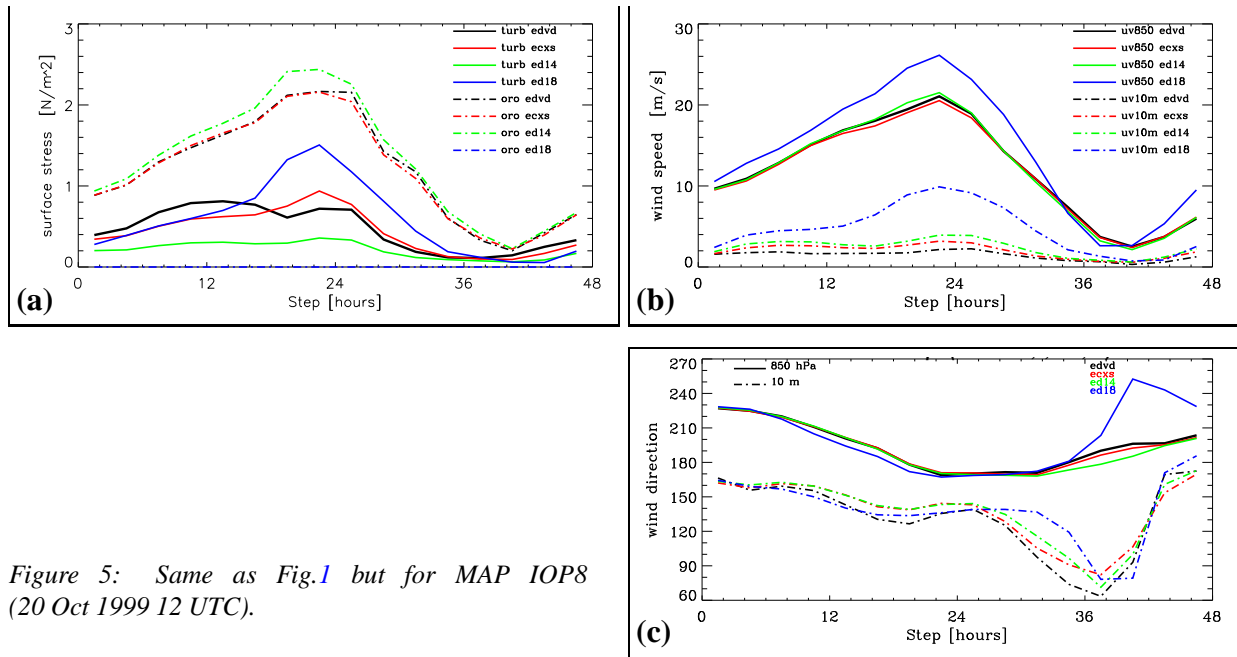


Figure 5: Same as Fig.1 but for MAP IOP8 (20 Oct 1999 12 UTC).

4.2 MAP IOP8

Integral values of turbulent and subgrid orography stress for the same mesoscale area ($45.5\text{--}47.5^\circ\text{N}$ and $7\text{--}14^\circ\text{E}$) show a similar behaviour as discussed for IOP2b: similar magnitude of surface stress caused by TOFD and GWD scheme using new and standard EFRL, a spin-up process of surface stress exerted by the new TOFD (exceeding the values exerted by the present scheme after 18 h), slightly higher low-level wind obtained with TOFD but similar wind speed in 850 hPa, and strong compensating effects of both drag schemes demonstrated with two sensitivity experiments (comp. Fig.5 with Fig.1).

However, there is a difference in the contribution of turbulent drag to the total surface stress. As stated above, different atmospheric conditions prevailed in the Alpine region during IOP2b and IOP8. During IOP8, when the troposphere was stably stratified and the flow was blocked, weaker low-level wind (averaged across the Alpine area amounting to 2 - 2.5 m/s for both standard and new) exert smaller TOFD surface stress than during IOP2b (when the area averaged mean low-level wind peaks in 3 - 4 m/s during unblocked flow conditions). Conversely, the surface stress generated by the GWD scheme compensates partly the weaker TOFD caused stress and is larger during IOP8. The TOFD generated surface stress contributes roughly 26 % to the total surface stress during IOP8 but about 37 % during IOP2b. The effect of boundary layer stability on turbulent form drag is further addressed in the next paragraph. Note that the wind shear in the stable boundary layer amounts to more than 30° during IOP8. Near the surface (10 m height) the wind direction prevails from SE to E, whereas at 850 hPa the wind comes from S on 21 Oct (area averaged values, Fig.5c). Using the new scheme turns the wind at 10 m height by about 10° in the clockwise direction.

For IOP8, both VHF and UHF observations were assimilated in the MAP re-analysis (Fig.6). Again, the key dynamical feature at Lonate during this episode is a jet passage between 21 Oct 00 UTC and 06 UTC attaining a wind velocity of more than 20 m/s above 3 km height. Within the lowest kilometre, a weak temporal fairly constant barrier wind is reanalyzed, above which the wind direction is veering towards S. Note the strong wind rotation from E to SW within 1 - 2 km height during the first half on 20 Oct, when the wind speed is very low, however. Above 2 km height, the wind is turning from WSW to SE in the course of the episode.

A satisfactory agreement is found for the first 18 hours of the short-range forecasts (20 Oct 12 UTC till 21 Oct 06 UTC) and re-analysis characterized by gradually increasing wind speed at all levels. Subsequently, all short-range simulations exaggerate the vertical extent of the jet forecasting wind speed exceeding 28 m/s within the lowest kilometre at 09 UTC on 21 Oct (Fig. 7). Shortly thereafter, the forecast wind weakens (to less than 8 m/s) below 5 km during the second half of 21 Oct underestimating the wind speed by more than 10 m/s. In terms of wind direction, the forecasts compare well with re-analysis until 21 Oct 12 UTC. Afterwards, the forecasts fail to predict the reanalyzed wind direction during a weak wind period. Again, intercomparing the three short-range forecasts shows slightly higher wind speed in the lowest kilometre for experiment using the new TOFD.

Overall, using MAP data to assess the impact of the new TOFD has only limited significance because of three reasons: firstly, the impact of the TOFD seems to be small and mainly limited to the lowest kilometre or two. Secondly, windprofiler data mainly detect the atmospheric flow only above this height with, thirdly, observation errors larger than the obtained impact itself. However, comparison of wind speed and direction with windprofiler observations and the MAP re-analysis data for the location of the Lonate instruments during two IOPs gives results which are in agreement with results obtained comparing cross-Alpine area averaged surface stress, wind speed and direction among different sensitivity experiments.

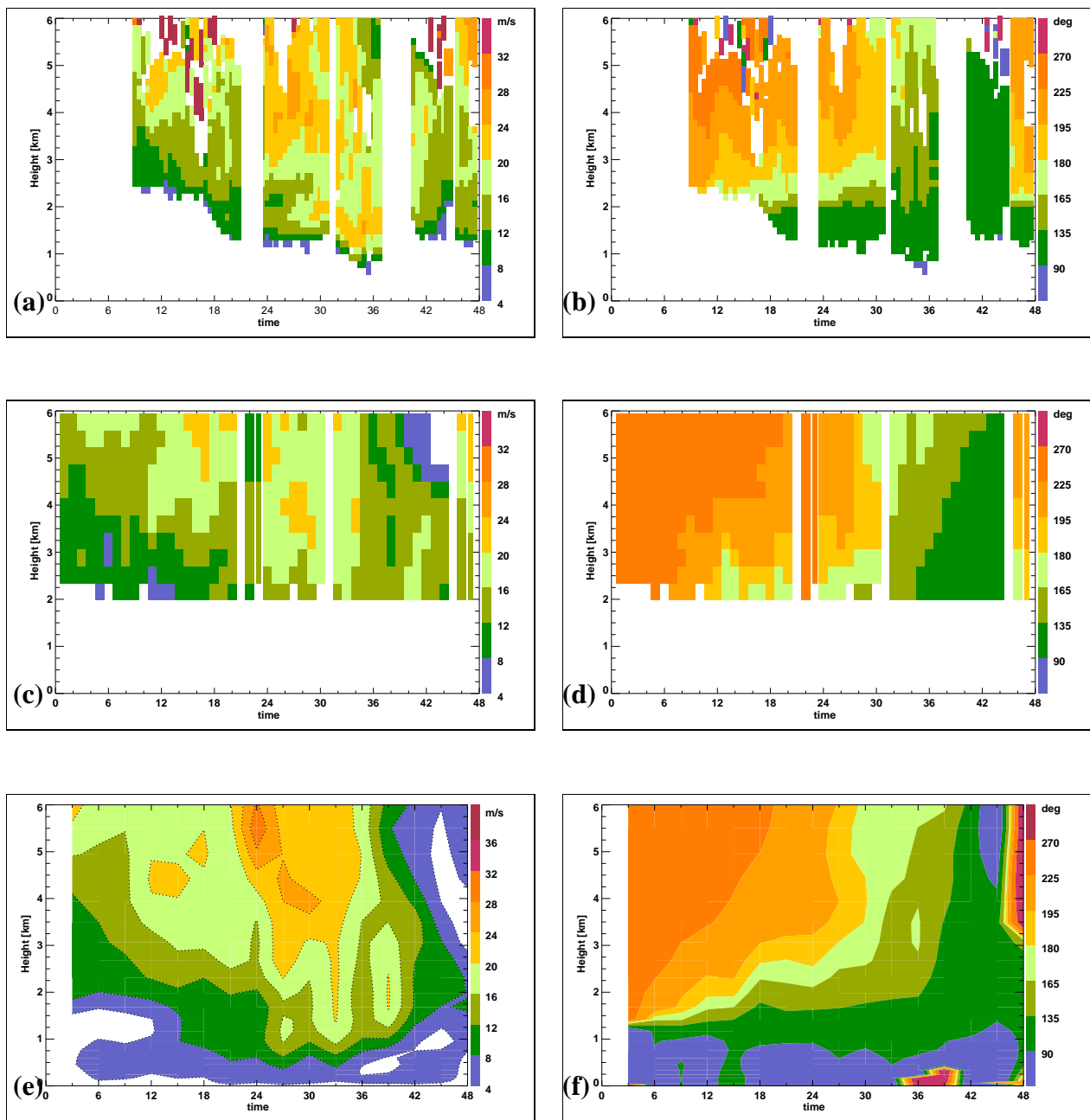


Figure 6: Time-height diagram (20 Oct 00 UTC till 22 Oct 00 UTC) of (a,c,e) horizontal wind velocity and (b,d,f) wind direction during IOP8. The observations by UHF windprofiler at Lonate are shown in (a,b), observations by VHF windprofiler in (c,d) and the corresponding analysis fields are shown in (e,f).

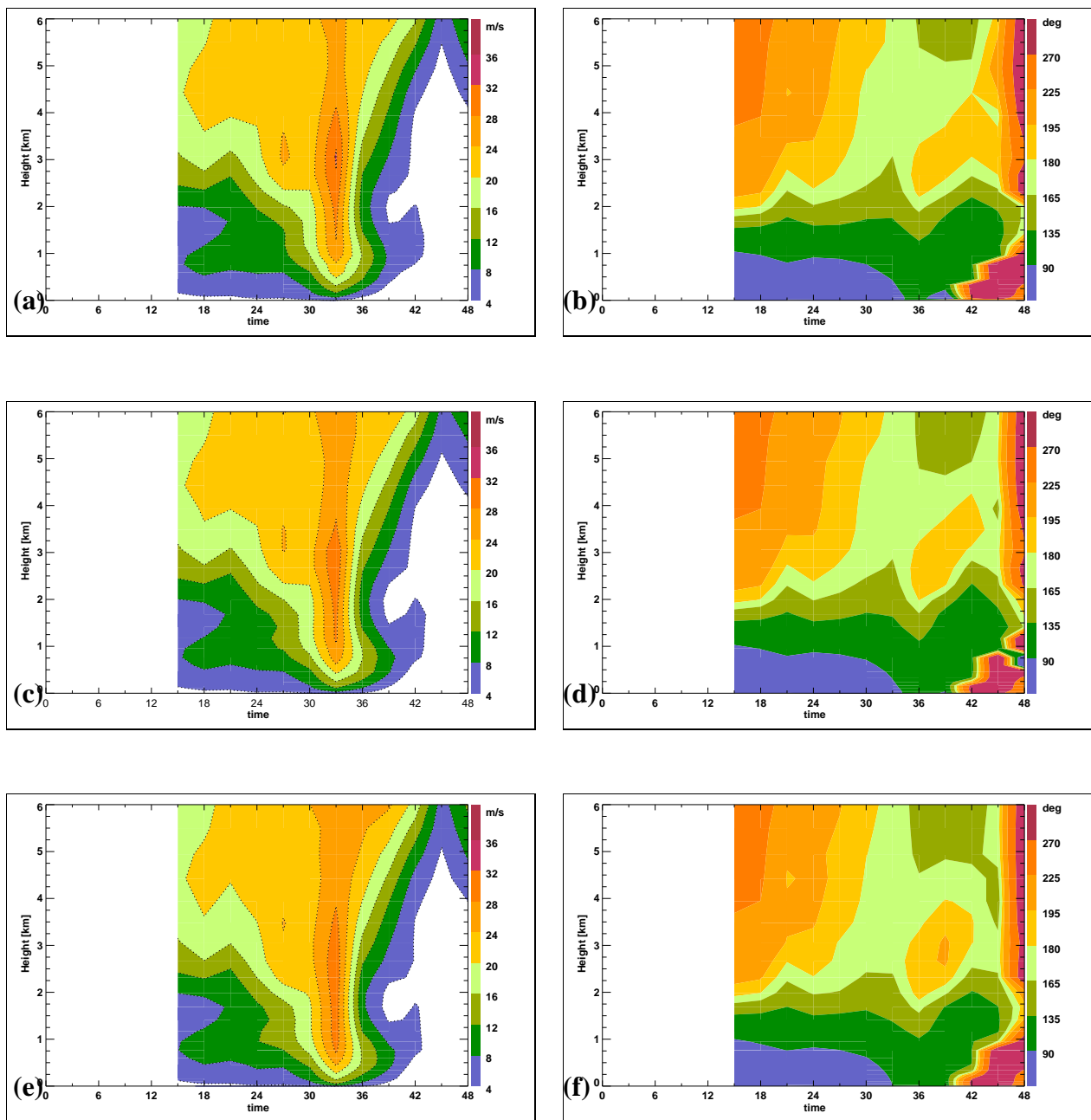


Figure 7: Time-height diagram (20 Oct 00 UTC till 22 Oct 00 UTC) of (a,c,e) horizontal wind velocity and (b,d,f) wind direction during IOP8 at Lonate: (a,b) CNTRL run using present EFRL (edvd), (c,d) new TOFD (ecxs) and (e,f) without TOFD (ed14).

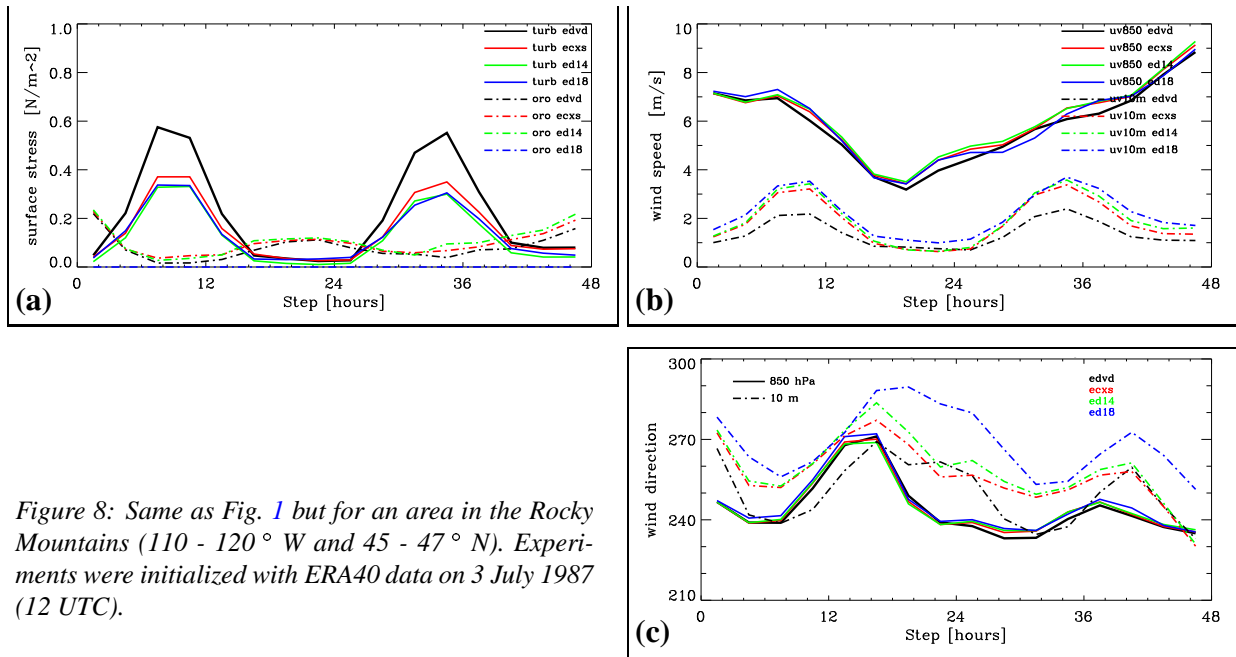


Figure 8: Same as Fig. 1 but for an area in the Rocky Mountains ($110 - 120^\circ$ W and $45 - 47^\circ$ N). Experiments were initialized with ERA40 data on 3 July 1987 (12 UTC).

4.3 The Rocky Mountains case

In order to further examine the effects of boundary layer stability on turbulent form drag, a set of short-range forecasts was conducted for a case-study characterized by an undisturbed diurnal cycle in the Rocky Mountains previously investigated by Beljaars (2001). There is evidence that the present effective roughness length scheme in the ECMWF model interacts very strongly with boundary layer stability and Beljaars et al. (2003) assume, that the new scheme is less modulated by stability.

In contrast to the previously discussed MAP cases, which are strongly driven by synoptic-scale forcing, this case represents fairly undisturbed diurnal cycles of the near surface wind speed and direction and the turbulent and subgrid orography stress (area averages over $110 - 120^\circ$ W and $45 - 47^\circ$ N, Fig. 8). Here, usage of the new TOFD shows a clear signal in the magnitude of the diurnal cycle. The daytime turbulent orographic surface stress is reduced by about 30% (red line), whereas the wind speed and direction close to the ground are increased by roughly 1 m/s and 15° , respectively. The subgrid orography scheme provides partial compensation for the weaker turbulent stress. However, during nighttime stable conditions there is hardly any impact noticeable.

Moreover, the small impact of both drag schemes on the overall model performance is remarkable. Switching the TOFD completely off, *i.e.* only drag of vegetation and GWD scheme is active, leads to very similar results (green lines) as using the new TOFD scheme. Without both TOFD and GWD schemes, the surface stress exerted by vegetation equals the total turbulent stress using new TOFD. However, there is no subgrid orography stress present in this case (blue lines).

With respect to the total surface stress, that is the sum of the vegetative, turbulent orographic and gravity-wave drag, the new scheme changes the contribution of the turbulent orographic drag. During stable conditions (Rocky Mountain case, MAP IOP8) the new TOFD scheme contributes about 10% less to the total surface stress whereas in unstable conditions (MAP IOP2b) the ratio of TOFD induced to GWD induced drag remains unchanged. To summarize, usage of the new scheme with its distributed drag reduces the diurnal amplitude of the turbulent stress but maintains the strong dependence on the stability.

5 Impact upon the model climatology

Two sets of six ensemble experiments have been performed for wintertime climate conditions in DJF87/88 and summertime conditions in JJA87. The large scale circulation by means of Z500 and Z200, the zonal mean wind speed and temperature, the zonal mean West-East surface stress and the zonal mean atmospheric blocking frequency are investigated to examine the response of the model climatology to the new TOFD.

5.1 Wintertime climate DJF87/88

Generally, the effect of the new TOFD on the large scale circulation is not very large as can be seen from the Z500 and Z200 fields and differences for Northern and Southern Hemispheres (Figs. 9 - 12).

Compared to ERA40 analysis, the large scale flow at 500 and 200 hPa in the Northern Hemisphere is too zonal using the new TOFD with the troughs across the Aleutes and Hudson Bay as well as the Rocky Mountains ridge being too weak (Figs. 9d and 10d). Using the standard EFRL, the trough across the Aleutes is even weaker, while the trough across the Hudson Bay is too deep (Figs. 9f and 10f), *i.e.* the large scale circulation is too much dominated by the Canadian trough. Direct comparison of both climate runs reveals a slightly superior behaviour using the new TOFD: upstream of the Rocky Mountains, the major mountain barrier between 40 - 60 ° N, the new scheme deepens the trough across the Aleutes and downstream it weakens the trough across the Hudson Bay (compared to the present scheme), clearly a beneficial impact of the new TOFD (Figs. 9b and 10b). Across Eurasia, there are only minor differences between both climate runs, showing slightly higher geopotential heights of Z500 and Z200.

Across the Southern Hemisphere, the differences between the new and the standard EFRL are only minor with lower geopotential heights across Antarctica using the new scheme (Figs. 11b). Both climate runs overestimate the trough upstream of the Patagonian Andes slightly. The underestimation of the geopotential heights across Antarctica in conjunction with the general overestimation between 40 - 60 ° S leads presumably to weaker zonal winds than in ERA40 (Figs. 11d,f). The geopotential height of Z200 of both climate runs is generally lower than in ERA40 (not shown).

Interestingly, the TOFD has hardly any impact on the large scale circulation, which can be deduced from Fig. 12a,c,d depicting the experiment without any TOFD scheme. Conversely, switching off both the TOFD and GWD schemes impacts highly on the global flow field by decreasing the geopotential across the Arctic and increasing it in mid-latitudes unrealistically (Fig. 12b,e,f).

Inspection of zonal mean flow and temperature is underlining the small but beneficial impact of the new TOFD. The jet structure of the north-hemispheric mid-latitude jet is improved, *i.e.* slightly smaller wind speed at the southern side of the jet and larger values at its poleward side (Fig. 13d). All climate experiments overestimate the wind speed at the southern side and underestimate it at the northern side of the mid-latitude jet, pointing towards a slight meridional displacement of the jet position (Fig. 13). The overestimation of the circumpolar wind is found to be weakest using the new TOFD. This is consistent with the stronger circumpolar flow deducible from the Z500 (Z200) patterns in Figs. 9d,f 10d,f and 12d. In total, experiment (ef01) using new TOFD shows best agreement with ERA40 analysis. The zonal mean temperature structure shows hardly any impact on the choice of the TOFD scheme. Compared to ERA40 analysis, all experiments tend to be too cold in the mid-latitude troposphere and too warm in the stratosphere (Fig. 14).

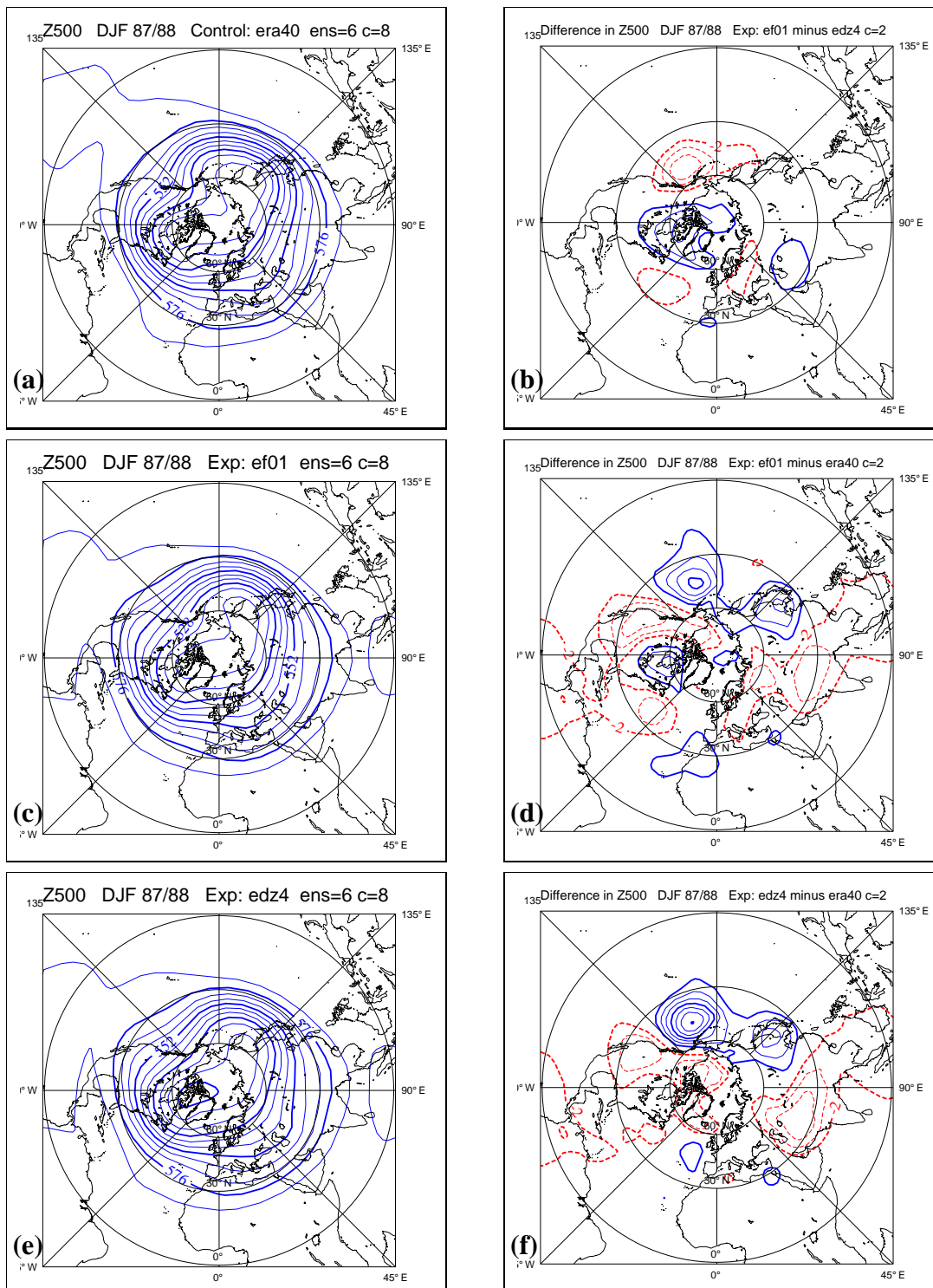


Figure 9: Mean 500 hPa height Northern Hemisphere verification for DJF 87/88 (contour interval: 8 dam for absolute fields and 2 dam for differences). The panels represent: (a) ERA40 analysis, (b) difference between experiments ef01 and edz4, (c) experiment with new TOFD (ef01), (d) difference between ef01 and ERA40 analysis, (e) control experiment using standard EFRL (edz4) and (f) difference between edz4 and ERA40 analysis.

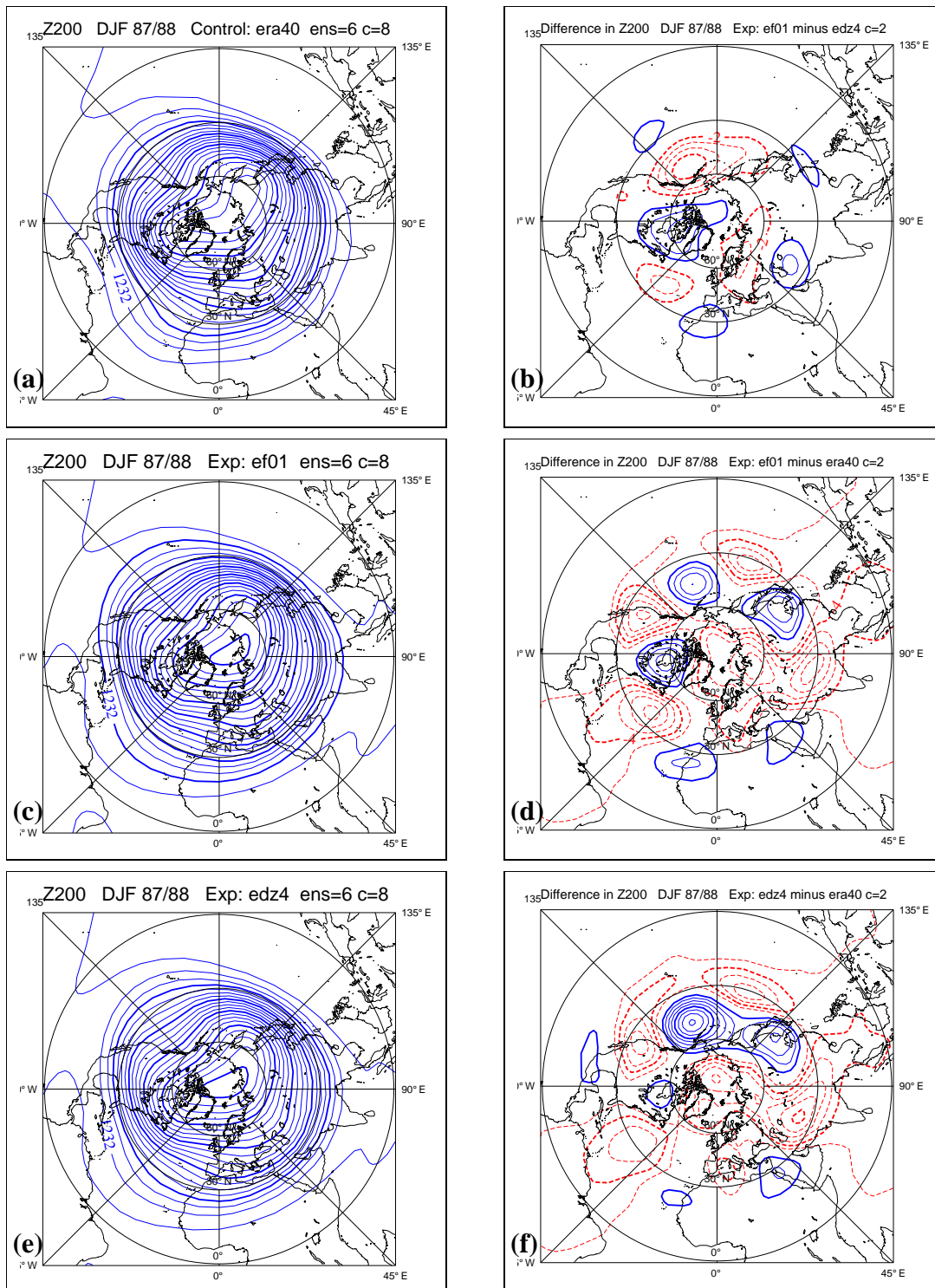


Figure 10: Same as Fig. 9 but for mean 200 hPa height Northern Hemisphere.

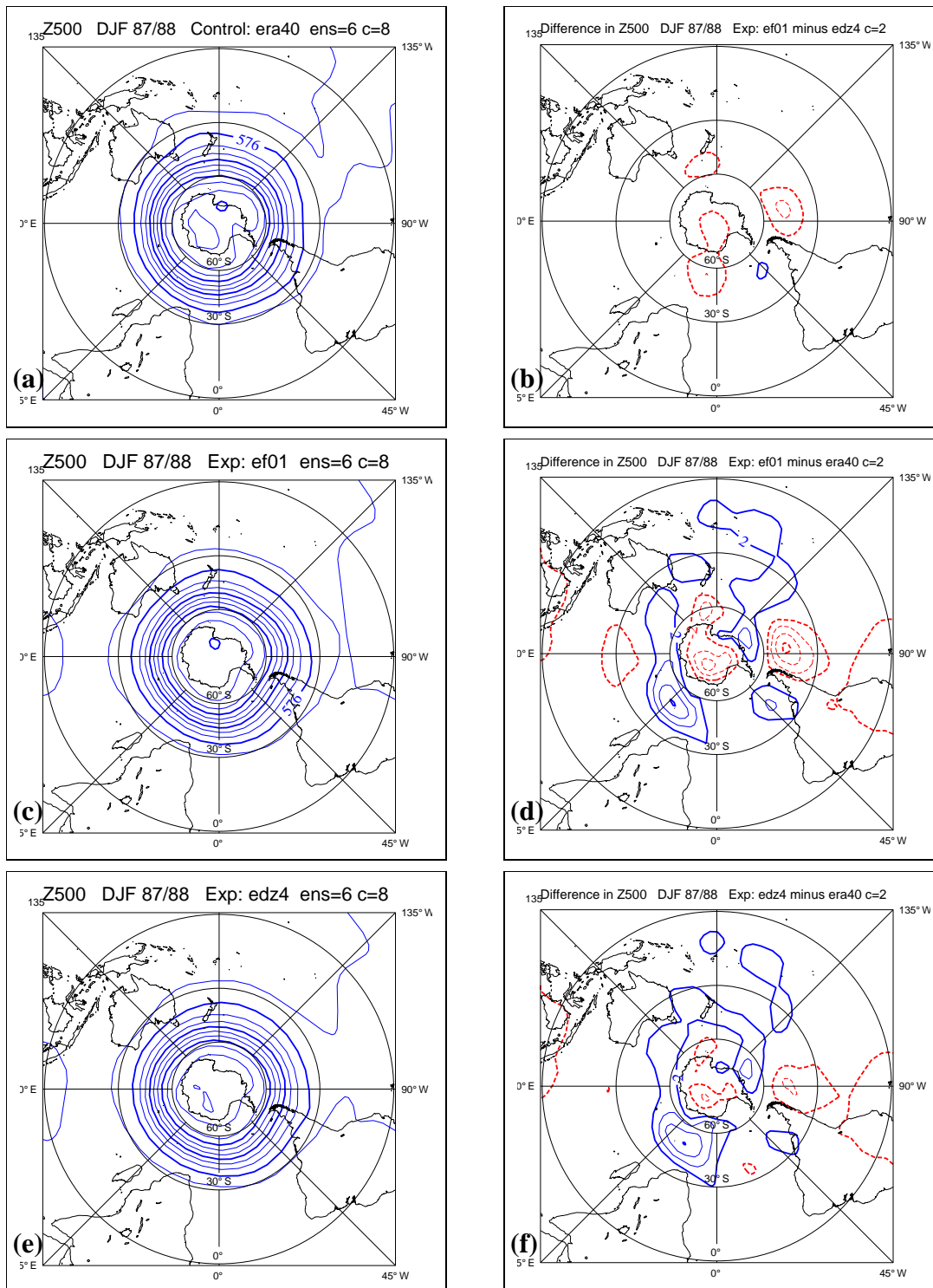


Figure 11: Same as Fig. 9 but for mean 500 hPa Southern Hemisphere.

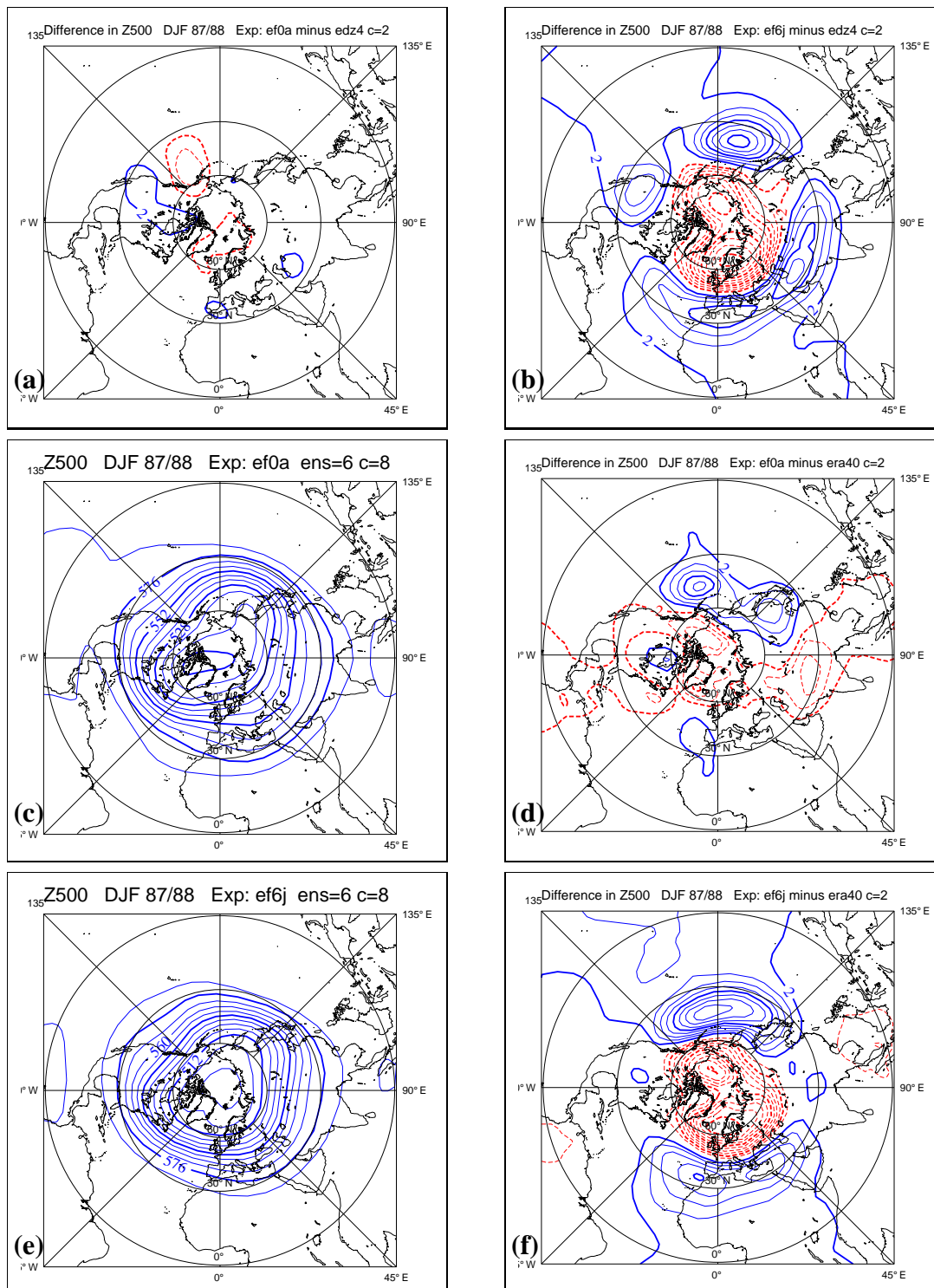


Figure 12: Mean 500 hPa height Northern Hemisphere verification for DJF 87/88 (contour interval: 8 dam for absolute fields and 2 dam for differences). The panels represent: (a) difference between experiments ef0a and edz4, (b) difference between experiments ef6j and edz4, (c) experiment without TOFD (ef0a), (d) difference between ef0a and ERA40 analysis, (e) experiment without both TOFD and GWD schemes (ef6j) and (f) difference between ef6j and ERA40 analysis.

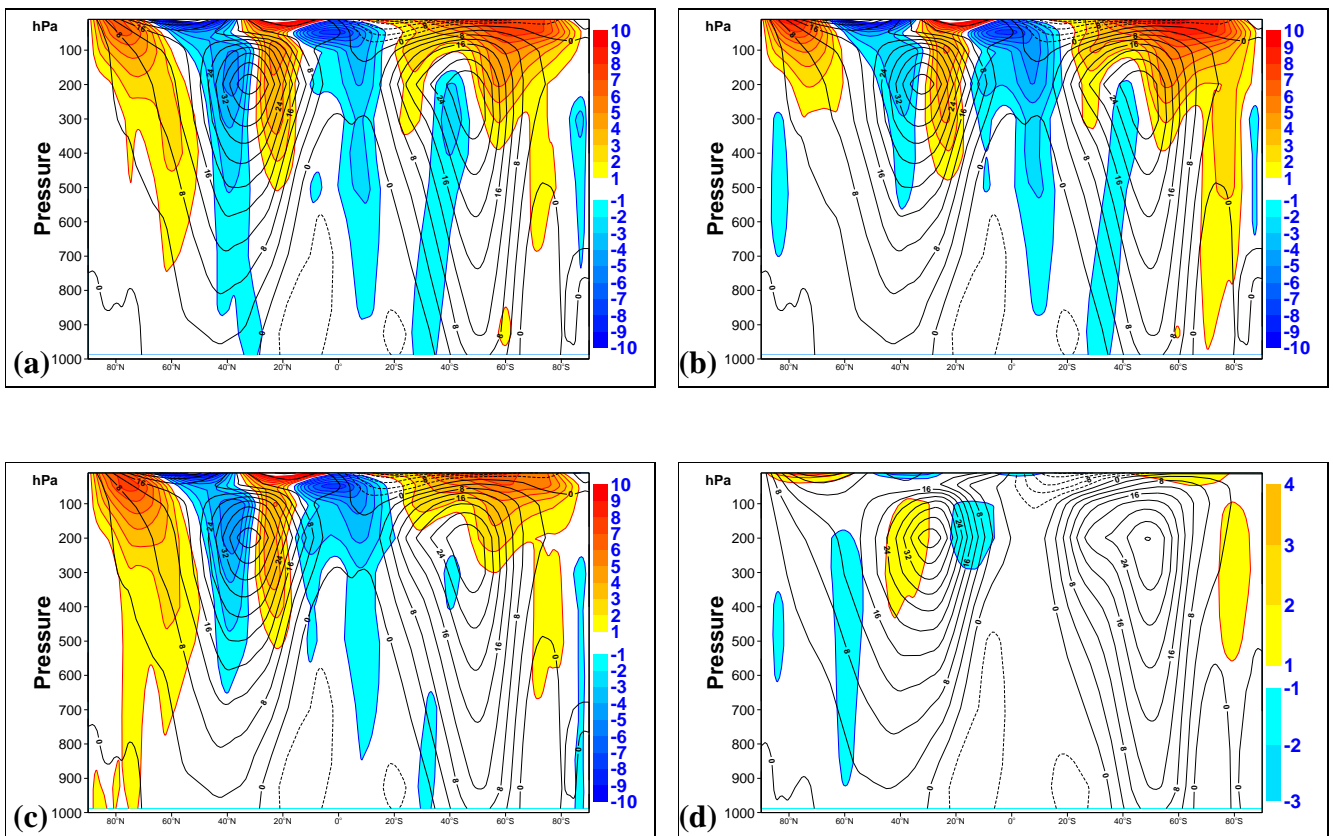


Figure 13: Zonal mean wind differences for DJF 87/88 displaying ERA40 analysis along with the difference between the following experiments and the verifying analysis (shaded): (a) control edz4, (b) experiment ef01 using the new parametrization, (c) experiment ef0a without a turbulent orographic form drag parametrization. In (d) the difference between experiment ef01 and control edz4 is shown.

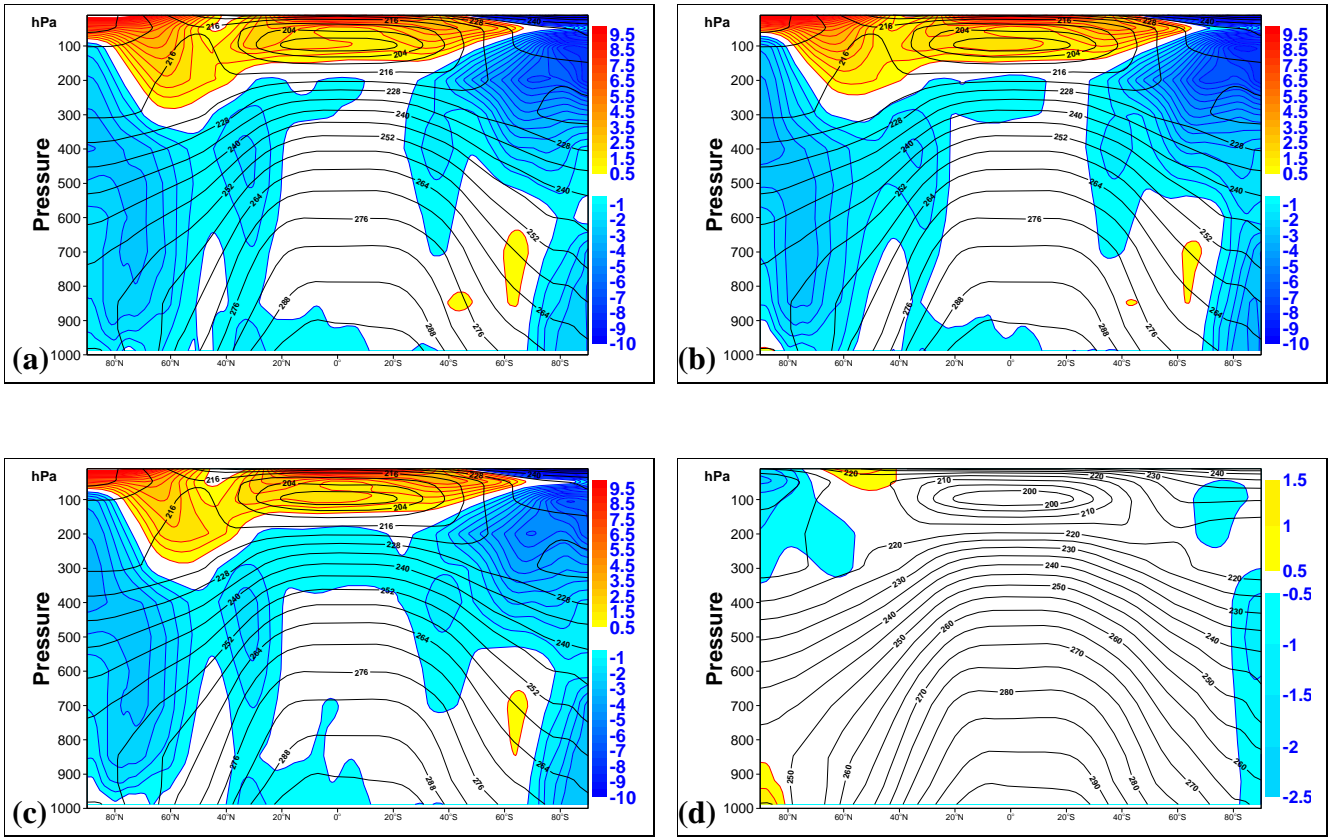


Figure 14: Same as Fig.13 but for temperature.

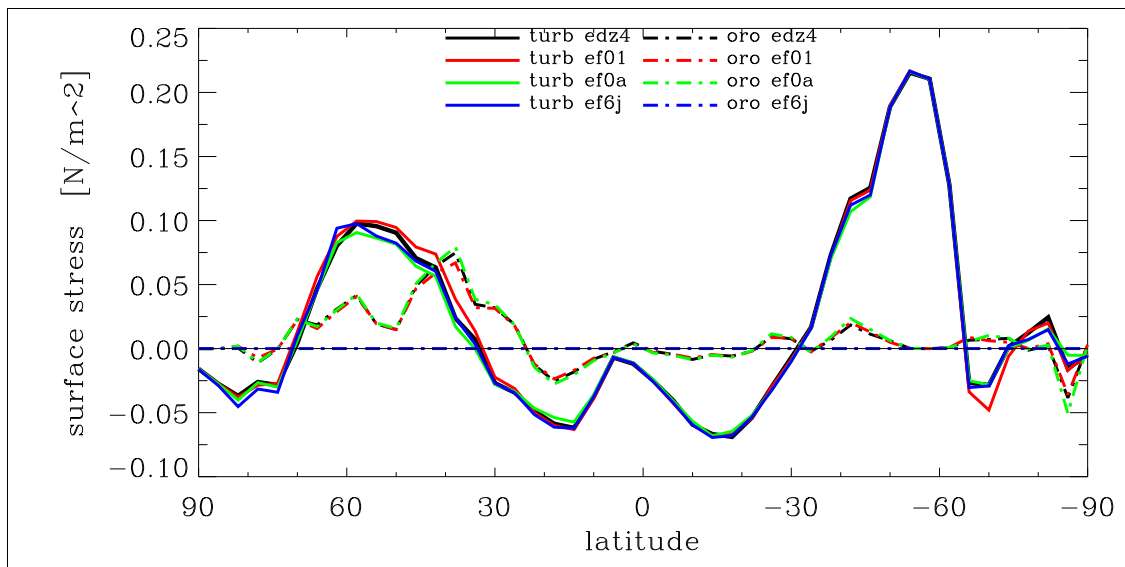


Figure 15: Zonal mean West-East stress from the turbulent drag scheme and the subgrid orography scheme for DJF 87/88. Four model versions are used: the standard EFRL (edz4) and the new (ef01) TOFD scheme. Additionally, an experiment (ef0a) without turbulent orographic drag scheme and one (ef6j) without both turbulent orographic drag and gravity wave drag scheme are displayed.

The zonal mean of West-East surface stress, caused by the turbulent and the subgrid orography drag, are shown for all wintertime climate experiments in Fig. 15. Using the new TOFD increases the zonal mean stress exerted by turbulent form drag in the mid-latitudes of the Northern Hemisphere slightly (red line). The compensation of the subgrid orography scheme becomes evident at 40° N, where the West-East GWD stress is slightly smaller than in the experiment using the standard EFRL. A decrease of drag in one scheme leads to increased surface wind which results in more drag from the other scheme. Note that the distribution of stress over land from the two schemes differs: the turbulent drag scheme is active everywhere, whereas the subgrid orography scheme is only active in case of stable stratification in areas with significant orography. Consequently, the surface stress from the subgrid orography scheme peaks in north-hemispheric mid-latitudes (Fig. 15). Another interesting feature is the stress maximum from the TOFD between $50 - 60^\circ$ S, caused by the strong wind in this oceanic region. Adjacent, the easterly surface stress exerted by the new turbulent form drag peaks at the Antarctic slopes (at 70° S). In summary, the surface stress is, as expected, strongly dependent on the prevailing wind speed and the new TOFD increases the stress exerted by turbulent form drag slightly. However, decreased stress from the subgrid orography scheme compensates this enhancement partly.

Finally, the atmospheric blocking frequency is investigated to assess the impact of the new scheme. Mountain drag is known to affect this parameter. In order to objectively describe atmospheric blocking the procedure described by Tibaldi and Molteni (1990) is applied. Basically, the geopotential height gradients at 500 hPa (interpolated onto a 4° by 4° regular latitude-longitude grid) are computed for every longitude point between $40^\circ - 80^\circ$ N. If the meridional gradient (from North to South over 20° latitude) is positive, the geostrophic wind in mid-latitudes is easterly and atmospheric blocking is present. However, it is a well-known shortcoming of many global circulation models, including the ECMWF model, that they underestimate the frequency of occurrence of atmospheric blocking (D'Andrea et al., 1998). Consequently, the focus in this study is on the qualitative differences among the climate simulations using different drag parametrizations. ERA40 analysis is given as reference.

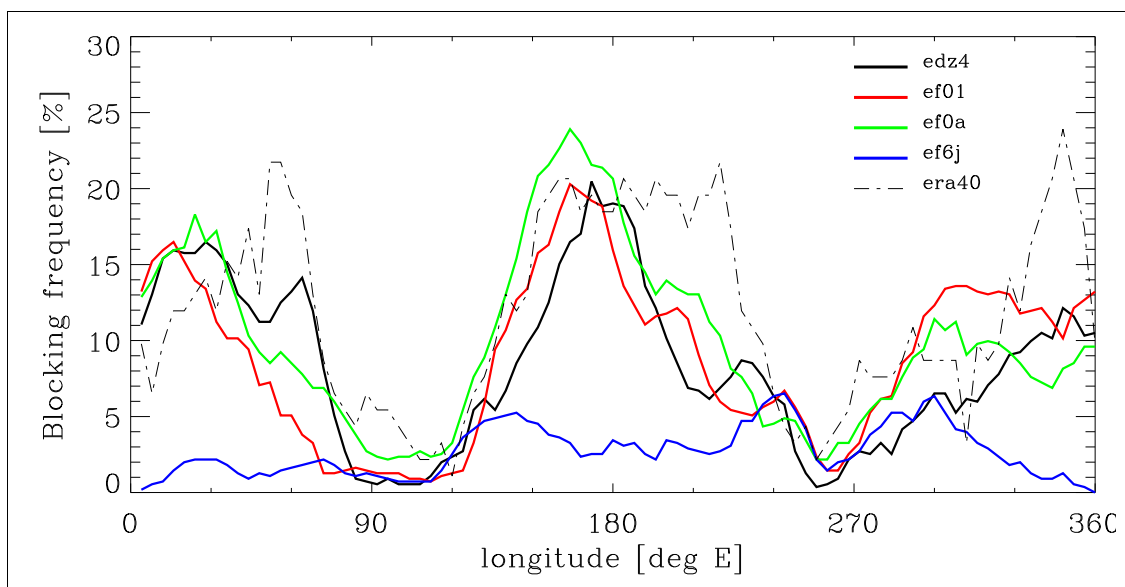


Figure 16: Frequency of wintertime days (DJF 87/88) that were classified as being blocked (%). Four model versions are used: the standard EFRL (edz4) and the new (ef01) TOFD scheme. Additionally, an experiment (ef0a) without turbulent orographic drag scheme and one (ef6j) without both turbulent orographic drag and gravity wave drag scheme are displayed.

For the single winter DJF87/88 all climate experiments (with GWD scheme; black, red and green lines in Fig. 16) reproduce the key feature, that is, two areas with enhanced blocking frequency in the North Pacific and the Euro-Atlantic region. At least for this winter season, the underestimation of the blocking frequencies (with respect to ERA40) is less dramatic as seen for the 40-year period 1962-2001 (Jung et al., 2003). Regarding the total of blocking events the impact of the new TOFD is nearly neutral, with a tendency to shift the blocking location slightly westward (red and black lines). The GWD scheme is the major element in determining atmospheric blocking conditions during the winter season (blue line depicting experiment ef6j without both drag schemes in contrast to green line displaying experiment ef0a without TOFD only).

5.2 Summertime climate JJA87

For completeness, some results of the summer climate experiments are depicted in this section. During summer, the depth of the polar vortex is much smaller than in winter (comp. Figs. 17 and 9). The impact of the new TOFD on the mean 500 hPa geopotential height is negligible (Fig. 17b). Both climate experiments (no data assimilation) generally underestimate the depth of the polar vortex (Fig. 17d,f). Conversely, in JJA the south-hemispheric polar vortex is deeper than in DJF and is slightly underestimated by the two climate runs, which hardly differ among each other (not shown).

Inspecting the zonal means of wind (Fig. 18) and temperature (not shown), again a small but favorable impact of the new TOFD is evident. As expected, the north-hemispheric mid-latitude jet is weaker than in winter. The differences (between new and standard EFRL) in the vicinity of the jet in the upper-troposphere (Fig. 18d) reduce the error of the climate run using the new scheme verified with ERA40 analysis (Fig. 18b). All climate runs overestimate the strength of the south-hemispheric jet.

For summer JJA87, the climate experiments reproduce the bimodal blocking frequency over the North Pacific and the Euro-Atlantic region (Fig. 19). Consistent with the 40-year mean (Jung et al., 2003), the blocking frequency is lower than that during winter. Compared against ERA40 analysis for JJA87, the climate experiments move the blocking maximum in the Euro-Atlantic region roughly 40 ° westward. Across the North Pacific, the flow simulated by climate experiment ef01 (using the new TOFD) is blocked in 20 % of the days. This blocking maximum compares well with ERA40 analysis but is shifted westward, again. The other climate experiments do not reproduce such a pronounced maximum over the North Pacific.

The fact that the subgrid orography scheme is only active in case of stable stratification in areas with significant orography becomes evident when comparing the blocking frequencies of the experiments with and without the GWD scheme (blue and green lines). During summer, when the atmosphere is more unstable, the contribution of the subgrid orography scheme to the blocking frequency is negligible and the main element is the turbulent vegetative (experiment ef6j) and orographic form drag.

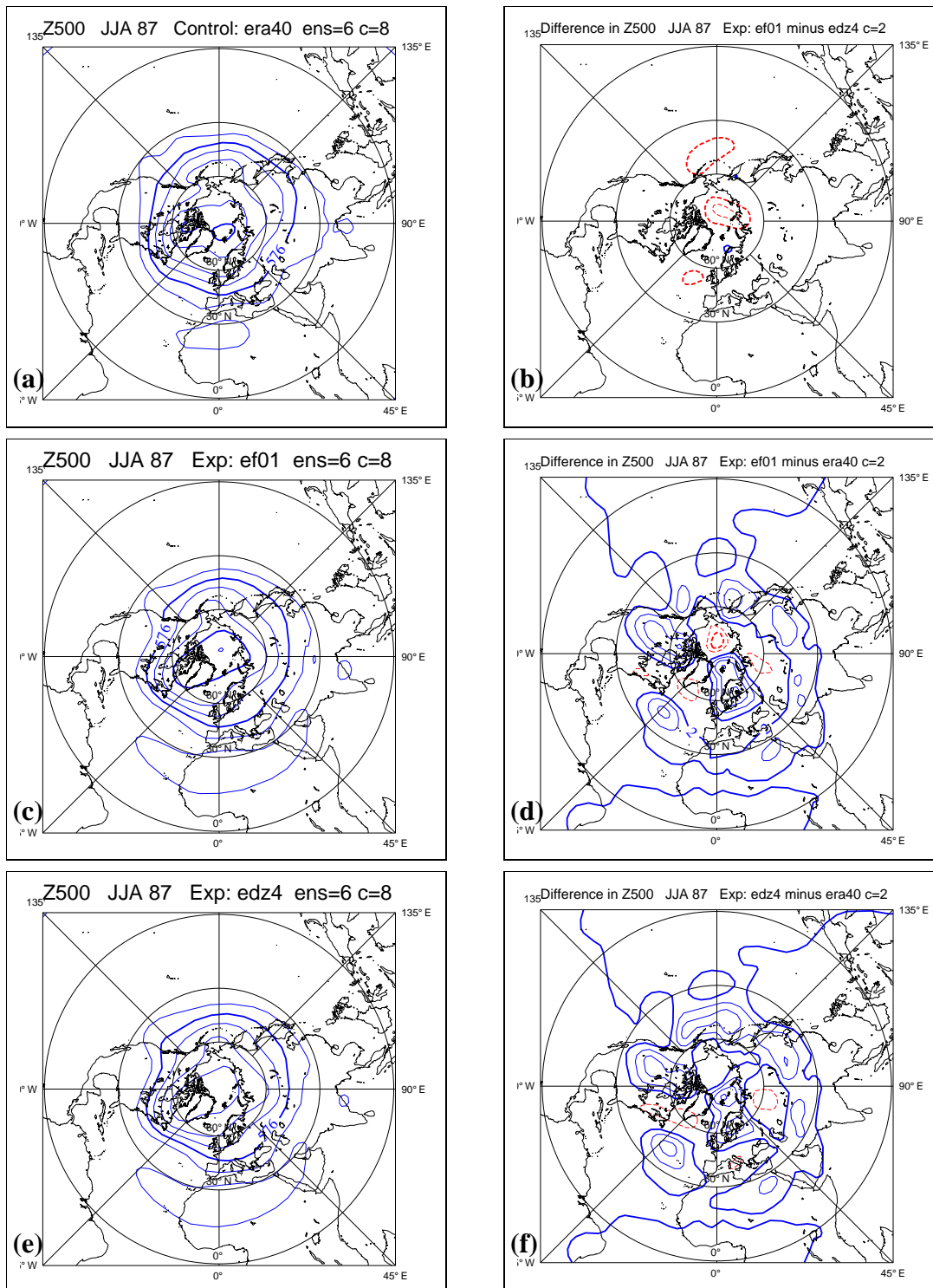


Figure 17: Same as Fig. 9 but for JJA87.

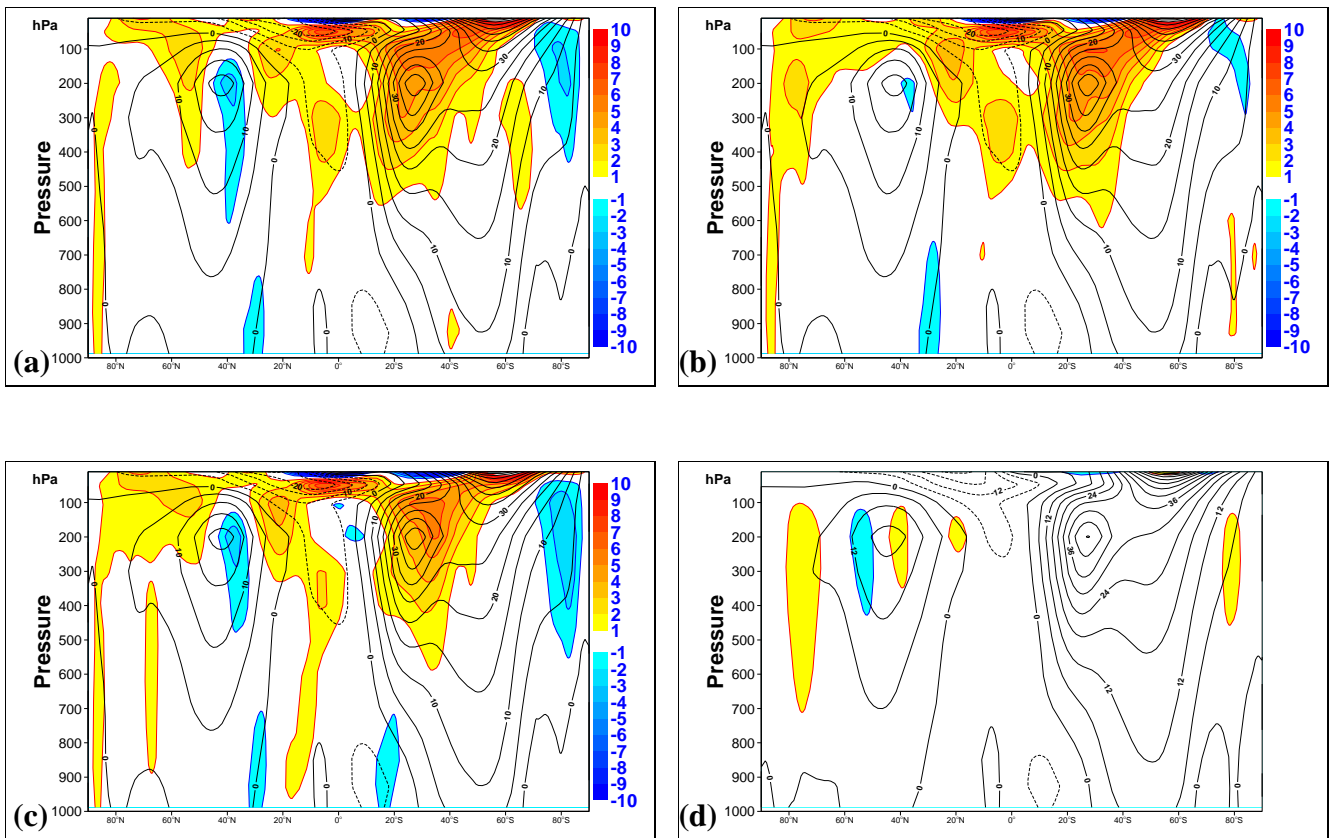


Figure 18: Zonal mean wind differences for JJA 87 displaying ERA40 analysis along with the difference between the following experiments and the verifying analysis (shaded): (a) control edz4, (b) experiment ef01 using the new parametrization, (c) experiment ef0a without a turbulent orographic form drag parametrization. In (d) the difference between experiment ef01 and control edz4 is shown.

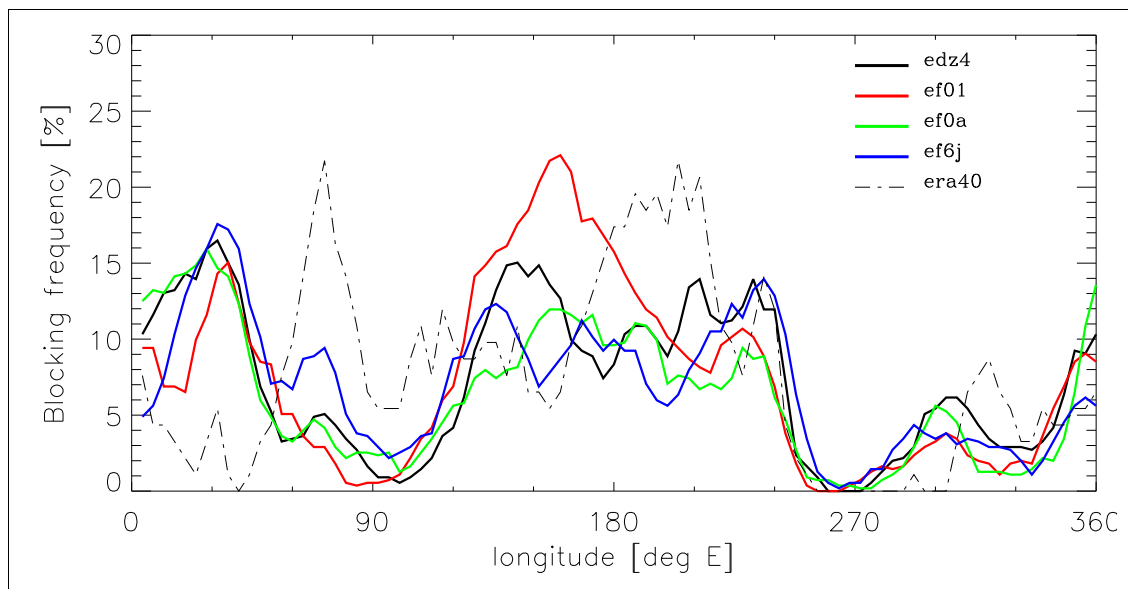


Figure 19: Same as Fig. 16 but for summertime days (JJA 87).

6 10-day forecast experiments

The final test examining the impact of the new turbulent orographic form drag scheme comprises a series of ten-day forecast experiments initialized between mid-January and mid-July 2003 every fourteen days. These forecasts were computed at operational T511L60 resolution and compared to ECMWF operations.

Once again, the scores of the anomaly correlation of the 500 hPa geopotential height surface using the new scheme show no degradation against ECMWF operations averaged over the 12 forecasts spread during the first 6 months of 2003 (Fig. 20).

Verification of 10 m-wind speed and direction with SYNOP observations is showing a minor impact of the new scheme (not shown). Daytime (+ 48 h fc) 10 m-wind speed compares slightly better with SYNOP observations across Europe, whereas the new scheme slightly deteriorates the near surface wind field during nighttime (+ 60 h fc). The wind direction is slightly overestimated using the new scheme. However, the spatial pattern of positive or negative increments seems to be correlated with the underlying vegetation type.

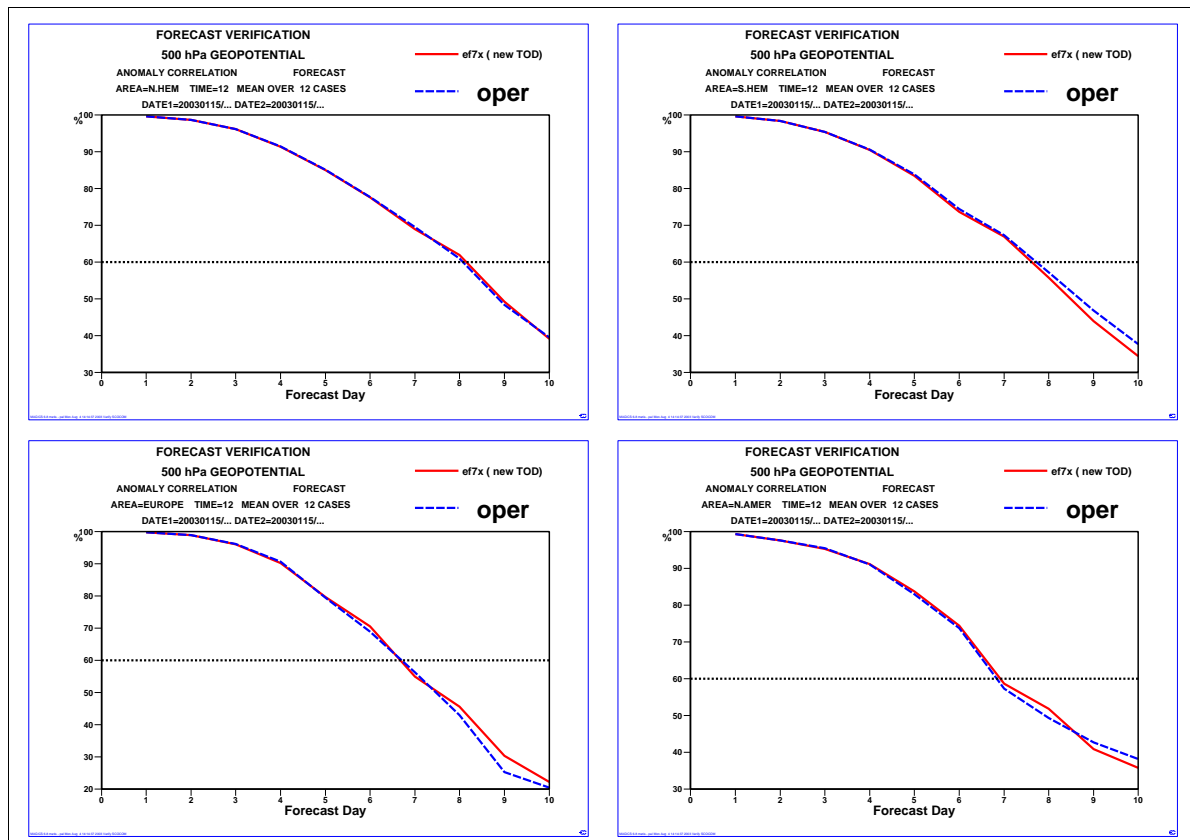


Figure 20: 500 hPa height anomaly correlation for different areas averaged over 12 forecasts spread over all seasons.

7 Conclusions and outlook

A new parametrization of turbulent form drag due to subgrid orography in large scale models has been evaluated performing a series of ECMWF forecast experiments. These are short-range case-study-type simulations of MAP IOPs, long integrations to assess the impact on the model climatology and finally a series of ten-day forecasts to be compared with operational scores.

Firstly, comparisons with the MAP re-analysis and windprofiler observations show a small increase in wind speed and direction within the lowest kilometres for two MAP IOPs using the new scheme. However, evaluating the results with MAP data has only limited significance since the impact is small (within the accuracy of the windprofiler observations) and confined to the lowest kilometres (where the windprofiler data is missing frequently). Intercomparison of cross-Alpine area averaged stress, wind speed and direction among different sensitivity experiments is confirming the slightly higher near surface wind, the weak impact on the total drag and the strong compensation between turbulent drag and gravity-wave drag. For a case-study in the Rocky Mountains characterized by an undisturbed diurnal cycle it is found that the new scheme with its distributed drag reduces the diurnal amplitude of the turbulent stress but retains the dependence on stability. The daytime turbulent orographic surface stress is reduced by about 30 %, whereas the wind speed and direction close to the ground are increased by roughly 1 m/s and 15 °, respectively.

Secondly, ensemble simulations performing long integrations to assess the impact on the model climatology (for DJF87/88 and JJA87) show a slightly superior behaviour using the new scheme with respect to ERA40 analysis. The small but beneficial impact is seen in the mean large scale circulation (by means of Z500 and Z200 for both hemispheres) and the zonal mean wind speed. It is found that the impact of the gravity-wave drag on the large scale flow is dominating the impact of the turbulent drag scheme. The zonal mean West-East surface stress is hardly changed by the new scheme. The turbulent drag scheme is dominating the subgrid orography scheme, which is only active in case of stable stratification in areas with significant orography, for most of the latitudes. Regarding the blocking frequency, the impact of the new TOFD during north-hemispheric wintertime is nearly neutral, with a tendency to shift the blocking location slightly westward. During the north-hemispheric summer season, the blocking frequency is lower than that during winter and the experiment using the new scheme reproduces a blocking maximum in the North Pacific verified with ERA40 analysis. In unstable conditions, the turbulent vegetative and orographic form drag are the main contributors causing blocking events.

Thirdly, a series of ten-day forecasts underlines the weak but beneficial impact of the new scheme by showing no degradation of scores (e.g. the anomaly correlation scores of the 500 hPa geopotential height) against ECMWF operations.

Thorough evaluation based on a series of various forecast experiments with the new scheme, in which the orographic form drag is vertically distributed, shows a slightly favorable impact. It is felt that the results provide the basis for incorporating the new scheme into data assimilation experiments and subsequently into ECMWF operations.

Acknowledgments

We thank Martin Köhler for his support concerning the climate simulations and Thomas Jung for providing the diagnostics to evaluate blocking events.

References

- Beljaars, A. C. M., A. R. Brown and N. Wood, 2003: A new parametrization of turbulent orographic form drag. Submitted to *Quart. J. Roy. Meteor. Soc.*, 21 pp.
- Beljaars, A. C. M., 2001: Issues in boundary layer parametrization for large scale models, in *Issues in parametrization of subgrid processes*, ECMWF seminar proceedings, Reading, England, pp. 71-87.
- Bougeault, P., P. Binder, A. Buzzi, R. Houze, J. Kuettner, R. B. Smith, R. Steinacker and H. Volkert, 2001: The MAP Special Observing Period. *Bull. Amer. Soc.*, **82**, 433–462.
- D’Andrea and co-authors, 1998: Northern Hemisphere atmospheric blocking as simulated by 15 atmospheric general circulation models in the period 1979-1988. *Clim. Dyn.*, **14**, 385-407.
- Grant, A.L.M. and P.J. Mason, 1990: Observations of boundary layer structure over complex terrain. *Quart. J. Roy. Meteor. Soc.*, **116**, 159–186.
- Jaubert, G. and J. Stein, 2003: Multiscale and unsteady aspects of a deep föhn event during MAP. *Quart. J. Roy. Meteor. Soc.*, **129**, 755-776.
- Jung, T. and A. Tompkins, 2003: Systematic model errors. ECMWF SAC-document, in preparation.
- Keil, C. and C. Cardinali, 2003: The ECMWF Re-Analysis of the Mesoscale Alpine Programme Special Observing Period. ECMWF Technical Memorandum 401. Available from ECMWF, Shinfield Park, Reading, RG2 9AX, UK.
- Lott, F. and M. Miller, 1997: A new subgrid-scale orographic drag parametrization: Its formulation and testing. *Quart. J. Roy. Meteor. Soc.*, **123**, 101-127.
- Mahfouf, J.-F., A.O. Manzi, J. Noilhan, H. Giordani, M. and Deque, 1995: The land surface scheme ISBA within the Meteo-France climate model ARPEGE, Part I: Implementation and preliminary results. *J. Clim.*, **8**, 2039-2057.
- Medina, S. and R. A. Houze Jr, 2003: Air motions and precipitation growth in Alpine storms. *Quart. J. Roy. Meteor. Soc.*, **129**, 345-371.
- Tibaldi, S. and F. Molteni, 1990: On the operational predictability of blocking. *Tellus*, **42A**, 343-365.
- Wood, N., A.R. Brown and F.E. Hewer, 2001: Parametrizing the effects of orography on the boundary layer, an alternative to effective roughness lengths. *Quart. J. Roy. Meteor. Soc.*, **127**, 759–778.